Published in partnership with Beijing Technology and Business University & International Union of Food Science and Technology



https://doi.org/10.1038/s41538-024-00341-3

Ginseng glucosyl oleanolate inhibit cervical cancer cell proliferation and angiogenesis via PI3K/AKT/HIF-1a pathway



Sitong Liu¹², Zhiyi Ai¹², Yue Hu¹², Guangquan Ren¹², Junshun Zhang¹², Ping Tang¹², Hongyang Zou¹², Xia Li¹², Yu Wang¹², Bo Nan¹² & Yuhua Wang¹², ≅

Ginseng (*Panax ginseng* C.A. Meyer) is widely used in several functional foods at present. Ginsenosides, is the most crucial bioactive constituents in ginseng whose antitumor activity have been widely reported. In this study, the effect of ginseng glucosyl oleanolate (GGO) produced from ginsenoside Ro through enzymatic transformation, on cervical cancer was evaluated in vitro and in vivo. GGO significantly inhibited the viability and colony forming ability of HeLa cells, and blocked the cell cycle in G0/G1 phase, which showed its ability to inhibit the proliferation of HeLa cells. GGO exhibited anti-angiogenesis effect in HUVECs, chick chorioallantoic membrane (CAM) and Matrigel plugs model. These effects were related to interference with the paracrine axis of VEGF/VEGFR2 and blockage of the downstream PI3K/AKT/HIF-1a signaling pathway of the autocrine axis. The dual inhibitory effects of GGO were also exhibited in immunocompromised mice undergoing heterograft and suppressed tumor growth without any side effects. These findings provide a theoretical basis for further development of GGO as a functional food with anti-tumor properties.

Ginseng (Panax ginseng C.A. Meyer) is a well-known medicine and food homology resource. In recent years as awareness regarding health and wellness has grown, it has gained remarkable popularity as functional food ingredient¹. Ginsenosides are the main active components in ginseng, which have been extensively reported for its biological activities including antiinflammatory, immune-stimulating, antiviral and anti-tumor². Currently, over 300 types of ginsenosides have been identified, and among them many ginsenosides (such as Rh2, Rg3, Rg5) exhibited various anti-tumor activities, including anti-proliferation and metastasis, induction of cell cycle arrest, inhibition of immune evasion and angiogenesis^{3,4}. Major ginsenosides can be metabolized into rare ginsenosides in vivo, which leads to different biological activities. For example, ginsenosides Rb1 can be metabolized into Rg3, Rh2, CK, F2, which played the role of anti-tumor, cardiac protection, and prevention of brain perfusion injury⁴⁵. Ginsenoside Ro is an abundant ginsenoside in ginseng, which is known for its anti-inflammatory activity, but there were fewer studies on its anti-cancer activity⁶. Notably, a previous study demonstrated that Ro did not have anti-tumor activity in vitro while its intragastric administration significantly inhibited tumor growth in vivo (b16f10 xenograft mice) through anti-angiogenesis⁷. This action was dependent on the active metabolites of Ro, as Ro did not possess antiangiogenic properties⁷. Nevertheless, it found that the bioavailability of Ro was extremely low, as only 10% of it was metabolized into Zingibroside R1, ChikusetsusaponinIVa, Calenduloside E, OA and GGO, while the remaining was excreted in urine and feces as Ro prototype8. Therefore, obtaining metabolites of Ro in in-vitro settings, and providing them readily usable in metabolized form for their biological activities is a significant approach towards health products of ginseng. GGO accounted for a high proportion in the metabolites of Ro (10%), which was difficult to obtain in vitro⁸. Our research team successfully obtained GGO through enzymatic transformation from ginsenoside Ro in vitro^{8,9}. It suppressed MAPK signaling phosphorylation and rebalanced gut microbiota to enhance shortchain fatty acid (SCFA) levels while ameliorating intestinal inflammation ultimately restraining tumor growth in nude mice9. However, the effect of GGO on other tumors has not been reported.

Cervical cancer is the second greatest cause of cancer-related death in developing nations and the fourth most common cancer among women

¹College of Food Science and Engineering, Jilin Agricultural University, Changchun, China. ²Jilin Province Innovation Center for Food Biological Manufacture, Jilin Agricultural University, Changchun, China. ³National Processing Laboratory for Soybean Industry and Technology, Changchun, China. ⁴National Engineering Research Center for Wheat and Cord Deep Processing, Changchun, China. —e-mail: yuhua-ww@163.com

globally¹⁰. Despite great advancements in current treatment approaches, such as aggressive surgery, chemotherapy, and neoadjuvant chemotherapy, the clinical outcomes for individuals with advanced cervical cancer are still not ideal¹¹. Studies have shown the pronounced heterogeneity of tumors, implying that a given compound may exert distinct mechanisms across different tumor types¹². Consequently, this study aimed to explore both the mitigating effects and specific mechanisms of GGO on cervical cancer progression, while concurrently exploring its potential as a functional food.

Results

Effect of GGO on the proliferation of HeLa cells

The chemical structure of GGO, which was produced via enzymatic transformation from ginsenoside Ro in vitro $^{\circ}$, was displayed in Fig. 1A. To assess the anti-cervical cancer efficacy of GGO in vitro, the MTT assay was conducted to elucidate the impact of GGO on the viability of HeLa cells. GGO (0.625–160 µg/mL) significantly inhibited the cell viability of HeLa cells and the IC50 values was 2.58 and 1.24 µg/mL at 24 h and 48 h, respectively (Fig. 1B). Colony formation occurs when a cell expands into a cluster of cells during proliferation. After treatment with GGO, the number of colonies decreased to 40.5–98.3% of the control group (Fig. 1C, E). Analyses of the cell cycle distribution via flow cytometry revealed that GGO induced the proportion of cells in the G0/G1 phase increased (Fig. 1D, F), which suggested that GGO arrested the cell cycle at the G0/G1 phase.

Effect of GGO on PI3K/AKT/HIF-1α signaling pathway in HeLa cells

PI3K/AKT/mTOR pathway is the most commonly dysregulated signaling pathway in human cancer that has a wide range of effects on basic cell functions, such as metabolism, proliferation and cell survival¹³. Therefore, the focus of this study was the connection between the inhibition of GGO on proliferation and the PI3K/AKT signaling pathway. GGO treatment significantly suppressed the phosphorylation of PI3K, AKT and mTOR in a dose-dependent manner under both normoxia and hypoxia conditions (Fig. 2A-D). Phosphorylation of PI3k/AKT is a necessary pathway for HIF-1α activation, which is an essential pathway for tumor cells to survive and proliferate in the low oxygen tension condition. It is well known that hypoxia is a prevalent hallmark in micro environment in many cancer types^{14,15}. Results of western blot analysis indicated that GGO inhibited the expression of HIF-1α under normoxia condition (Fig. 2A, C), and reversed the upregulation induced by hypoxia (Fig. 2B, D). When the concentration of GGO reached 40 µg/mL, the inhibition rate reached more than 50%. Immunofluorescence results showed that GGO inhibited the nuclear translocation of HIF-1a induced by hypoxia (Fig. 2E). These results suggested that GGO inhibited HeLa cell proliferation probably by inhibiting PI3K/AKT signaling phosphorylation and HIF-1α nuclear translocation.

GGO inhibited VEGF through the PI3K/AKT/HIF-1α pathway in HeLa cells

Vascular endothelial growth factor (VEGF) is one of the most essential growth factors to promote cancer angiogenesis, and regulated by HIF- $1\alpha^{16}$. Western blot results exhibited that GGO inhibited the expression of VEGF under both normoxia and hypoxia condition (Fig. 3A and B). Interestingly, GGO intervention did not further decrease the expressions of p-PI3K, HIF-1 α and VEGF in HeLa cells, when pre-treated with PI3K inhibitor LY294002 (Fig. 3C). Pretreatment with HIF-1a inhibitor LW6 resulted in the decreased expressions of HIF-1α and VEGF decreasing, compared to the control group (Fig. 3D). There were no significant changes in VEGF expression in the GGO (20 µg/mL) combined LW6 treatment group compared to LW6 group (Fig. 3D). These results indicated that GGO inhibited the expression of VEGF by blocking PI3K/AKT/ HIF-1α pathway. The process of angiogenesis is regulated by many proangiogenic factors, and other pro-angiogenic factors (VEGF, FGF, EGF and PDGF) secreted by HeLa cells, which were detected by enzyme linked immunosorbent assay. Surprisingly, GGO treatment significantly decreased the secretion of VEGF to 65.5-86.6% of control group (Fig. 3F), while there were no significant changes observed in the secretions of PDGF, FGF and EGF (Fig. 3E, G, H).

GGO inhibited the process of angiogenesis in HUVECs by interfering VEGF/VEGFR2 paracrine pathway

Endothelial cells proliferation, migration, invasion and tube formation play important roles in the process of angiogenesis¹⁷. Firstly, GGO (20-80 µg/mL) significantly decreased the cell viability of HUVECs induced by VEGF at 24 h (Fig. S1B). While no significant alterations in the viability of HUVECs treatment without VEGF or the level of LDH released by HUVECs were observed, suggesting that GGO did not induce toxic effects on HUVECs (Fig. S1A, C). In wound-healing assay, a substantial number of cells migrated to the gap following VEGF treatment and resulted in a reduction in wound area to 36.6% of control group. The wound area increased to 42.4-113.4% of the control group after treatment with both GGO and VEGF (Fig. 4A, D). Similarly, the invasive cell count increased to 179.8% of the control group following VEGF treatment and decreased to 31.5-160% of the control group when treated with both GGO and VEGF (Fig. 4B, E). VEGF-induced HUVECs exhibited superior tubular structures compared to the control group; however, intervention with both GGO and VEGF gradually disrupted endothelial tubes and significantly reduced branch points (Fig. 4C, F). As a well-known mediator in cancer-related angiogenesis, VEGF predominantly exerts its biological effects by activating VEGFR2¹⁸. Western blot results showed that GGO reduced the phosphorylation level of VEGFR2 and the expressions of its downstream matrix metalloproteinase (mmp2 and mmp9) in HUVECs induced by VEGF (Fig. 4G). These effects were important for the migration, invasion, and tube formation in HUVECs induced by VEGF, which were evaluated in this study. These findings suggest that GGO exerts its anti-angiogenic effect by interfering with the VEGF/VEGFR2 paracrine axis (Fig. S1D).

GGO blocked VEGF/VEGFR2 autocrine axis by activating Spry2 in HeLa cells

Studies have found that VEGF/VEGFR2 autocrine pathway exists in cervical cancer, that can catalyze the phosphorylation of PI3K/AKT signaling pathway, thereby playing a variety of roles, including promoting cell proliferation and angiogenesis¹⁹. Spry2 acts as a negative regulator of the VEGFR2 downstream signaling by enhancing the phosphatase and tensin homolog (PTEN) stability²⁰. Western blot results demonstrated that GGO significantly increased the expressions of Spry2 and PTEN, and significantly decreased the phosphorylation of VEGFR2 (Fig. 5A). The relationship between the inhibitory effect of GGO on the PI3K/AKT pathway and its ability to induce Spry2 activation was confirmed through siSpry2 transfection assay. The optimal concentration of siSpry2 (50 pmor/L) was determined by pre-experimental screening (Fig. S1B). As anticipated, the expressions of p-PI3K, p-AKT, p-mTOR, HIF-1a and VEGF were significantly increased in the group silenced Spry2, whereas the expression of PTEN was significantly suppressed. Surprisingly, the above situation was not significantly changed after GGO (20 µg/mL) intervening (Fig. 5B, C). According to the above findings, it was evaluated that GGO blocked the PI3K/AKT signaling pathway by activating Spry2, thereby inhibiting VEGF/VEGFR2 autocrine in HeLa cells (Fig. 5F). In order to determine the effect of changes in VEGF/VEGFR2 autocrine axis in HeLa cells on their ability to induce angiogenesis, conditioned media of HeLa cells treated in different ways were collected to culture HUVECs. The results revealed that the conditioned media (CM) from HeLa cells induced the tube formation of HUVECs; however, this ability was abolished when HeLa cells were pre-treated with GGO at a concentration of 20 μg/mL. In addition, HUVECs exhibited strong tube forming capability when cultured in the CM from HeLa cells which were silenced Spry2 and treated with or without GGO (20 µg/mL) (Fig. 5D, E). These results indicated that blockage of the VEGF/VEGFR2 autocrine axis was an important pathway for GGO to simultaneously inhibit proliferation of HeLa cells and angiogenesis of HUVECs.

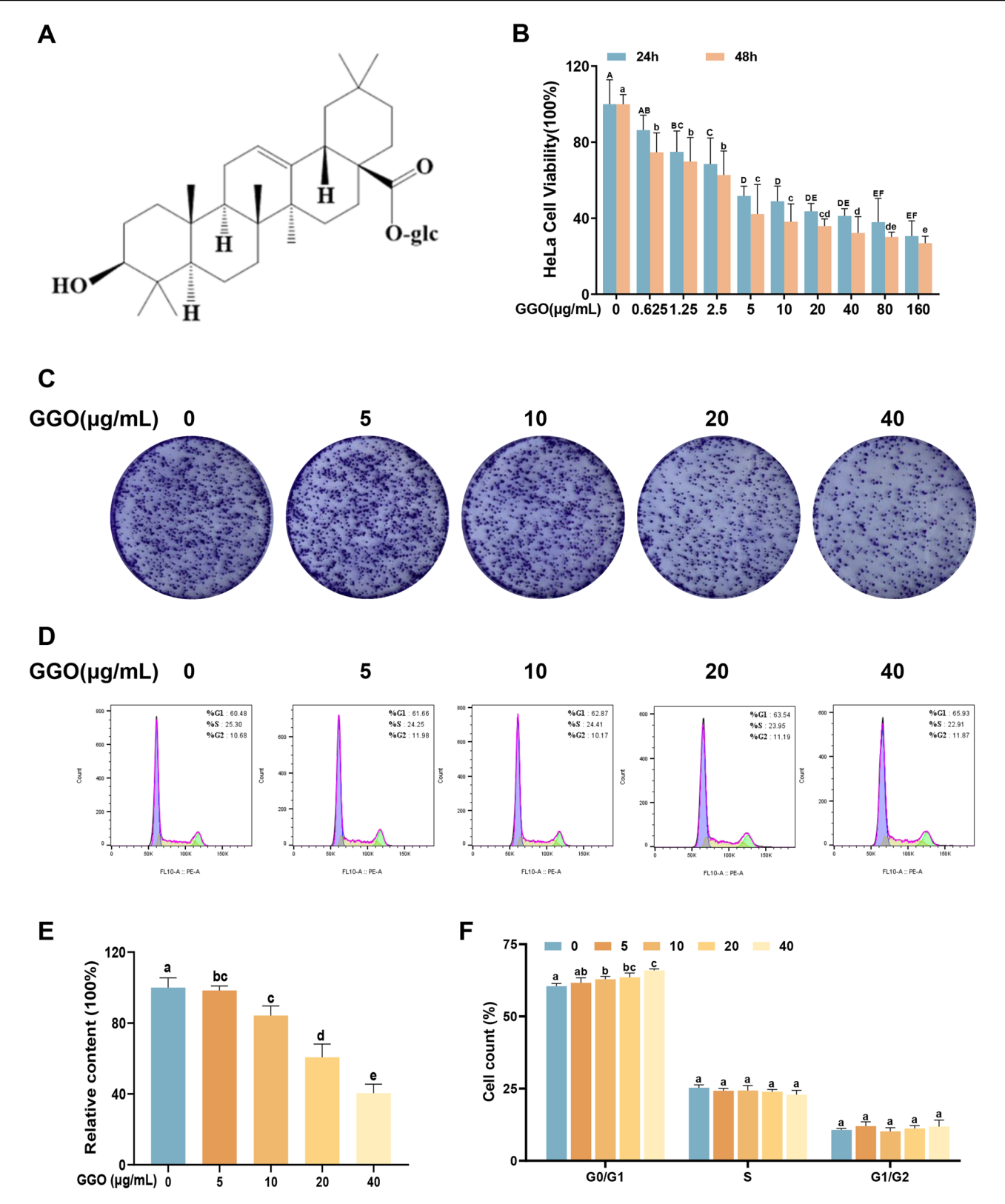


Fig. 1 | Effect of GGO on the proliferation of HeLa cells. A Chemical structure of GGO. B Effects of GGO on HeLa cells proliferation determined by the MTT assay. C Colony forming ability of HeLa cells following treatment with GGO. D Flow cytometry results showed the cell cycle distribution of HeLa cells treated with GGO.

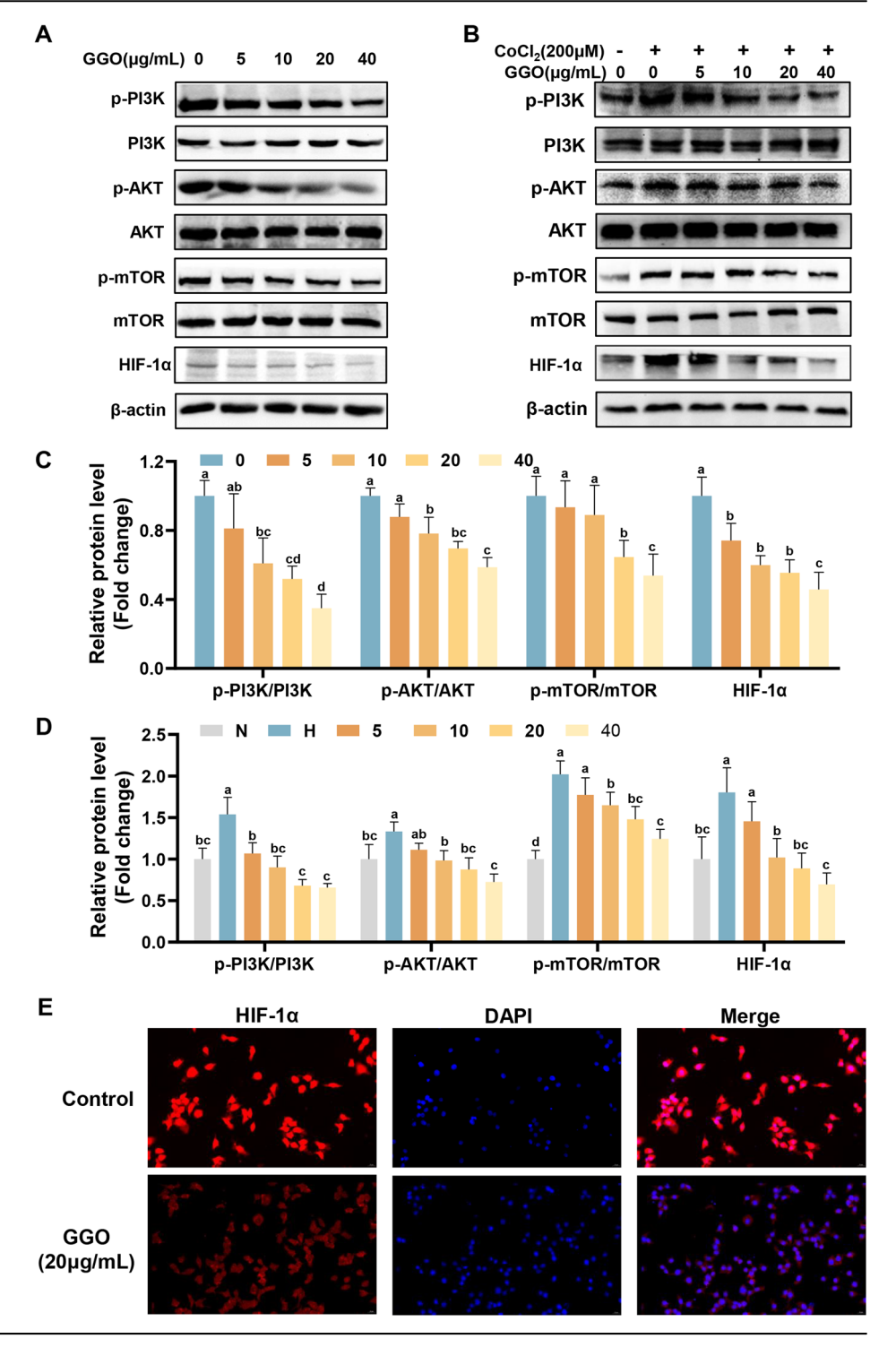
The corresponding statistical analysis of (E) colony formation and (F) cell cycle distribution. Values were represented as means \pm SD (n = 3). Different letters indicated the significant differences between different groups (p < 0.05).

Effects of GGO on angiogenesis in vivo

The anti-angiogenic effect of GGO in vivo was assessed using the CAM and Matrigel plug assay, which are excellent models for studying the tumor angiogenesis. Matrigel plugs loaded with VEGF

became dark red, indicating abundant microvessel formations. However, those Matrigel plugs loaded with both VEGF and GGO exhibited a pale red and were nearly transparent, suggesting that the microvessel formation was impeded (Fig. 6A). Hemoglobin

Fig. 2 | Effect of GGO on PI3K/AKT/HIF-1α signaling pathway in HeLa cells. The expressions of p-PI3K, PI3K, p-AKT, AKT, mTOR, p-mTOR and HIF-1α in HeLa cells following treatment with GGO under (**A**) normoxia and **B** hypoxia conditions. **C**, **D** The relative intensities of these protein bands were analyzed by the ImageJ software, β -actin served as a loading control. **E** Immunofluorescent staining of HIF-1α in HeLa cells following treatment with GGO (0 and 20 μg/mL) under hypoxia condition. Scale bar, 20 μm. Values were represented as means \pm SD (n = 3). Different letters indicated the significant differences between different groups (p < 0.05).

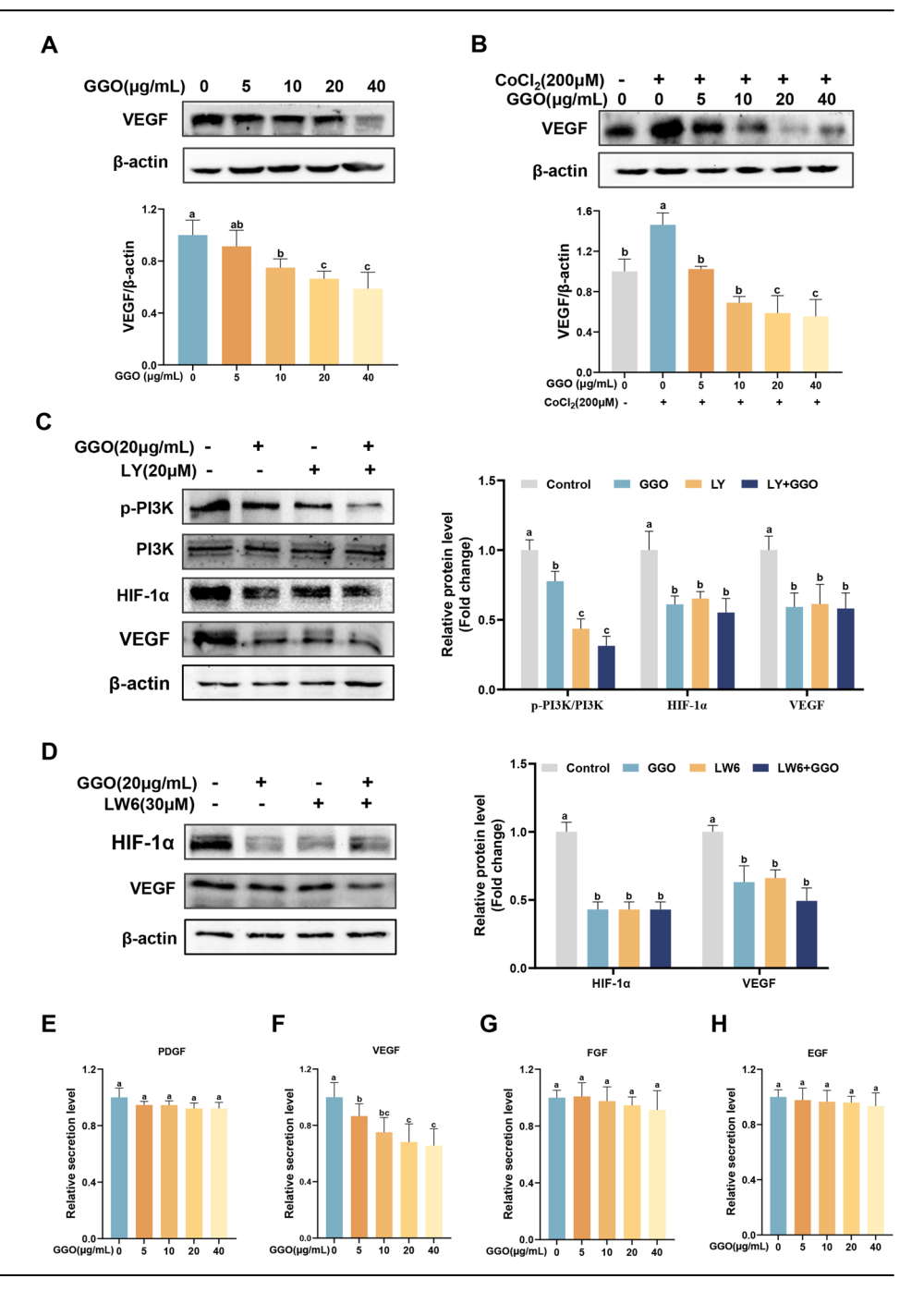


concentrations were assessed to quantify the formation of microvessel. Surprisingly, the hemoglobin levels in the VEGF-induced group were almost 14 times of the control group. Compared to the VEGF-induced group, hemoglobin levels decreased by 40.09% and 75.11% in groups treated with GGO (400 μ g/mouse or 800 μ g/mouse) combined with VEGF (Fig. 6B). Microvessel density significantly increased by 54.0% in VEGF-induced CAM compared to the control group, while treatment with both GGO and VEGF resulted in a decrease of microvessel density by 29.79–69.33% compared to the VEGF-induced group (Fig. 6C, D).

Effects of GGO on tumor growth in vivo

The anti-tumor efficacy of GGO in vivo was investigated using the HeLa xenograft mouse model. Treatment with GGO at doses of 40 and 80 mg/kg for 28 d significantly inhibited the final tumor volume (Fig. 7B, C). Immunohistochemistry assay was employed to examine the expressions of CD31, an endothelial marker, and VEGF in tumor tissues. As shown in Fig. 7D, the tumor sections from control group mice exhibited abundant VEGF and CD31-immunopositive cells, but in contrast, tumor sections from GGO-treated group mice exhibited less VEGF and CD31-immunoreactive cells. The levels of VEGF in serum were significantly reduced after GGO

Fig. 3 | GGO inhibited VEGF through the PI3K/ AKT/HIF-1α pathway in HeLa cells. The expression of VEGF in in HeLa cells following GGO treatment under (A) normoxia and (B) hypoxia conditions. C The expressions of PI3K, p-PI3K, HIF-1α and VEGF in HeLa cells pre-treatment with PI3K inhibitor (LY294002, 20 µM) and combined with or without GGO (20 µg/mL). D The expressions of HIF-1α and VEGF in HeLa cells pretreatment with HIF-1α inhibitor (LW6, 30 μM) and combined with or without GGO (20 µg/mL). The relative intensities of these protein bands were analyzed by the ImageJ software, β-actin served as a loading control. The inhibition of GGO on secretion of (E) PDGF; (F) VEGF; (G) FGF and (H) EGF were detected using ELISA kits. Values were represented as means \pm SD (n = 3). Different letters indicated the significant differences between different groups (p < 0.05).



treatment (Fig. S1F). Excitingly, after GGO intervention, there were numerous hemorrhagic foci and cell disruptions within the tumor, but none in the normal tissue, suggesting that GGO targeted to tumor blood vessels and had no toxic effect on normal tissues (Fig. 7D and S2). In addition, GGO treatment significantly decreased the phosphorylation levels of VEGFR2, PI3K, AKT and mTOR in tumor tissues of the Hela xenograft mice, which was consistent with the results in vitro (Fig. 7E). In conclusion, GGO exhibited remarkable anti-angiogenic properties in vivo, thus inhibiting the malignant progression of tumors.

Discussion

Ginseng has become an important dietary supplement for preventing and treating cancer. Surveys indicated a significant association between ginseng consumption and reduced cancer risk (lung, gastric, colorectal, breast, and prostate)²¹. This therapeutic potential was attributed to its primary bioactive compounds, ginsenosides (Rk3, CK, Rg3, Rg5, Rh2), with Rg3 and Rh2 have

been approved as antitumor drug and health product, respectively^{1,22}. However, previous studies mainly focused on protopanaxadiol type (PPDtype) or protopanaxatriol type (PPT-type) ginsenosides, with less attention given to oleanolic acid type (OA-type) ginsenosides⁴. Ro is an abundant OAtype ginsenoside with no antitumor activity in vitro, but inhibited tumor growth in vivo due to its metabolites7. Our research group successfully obtained GGO from ginsenosides by enzymatic transformation in vitro, which is an important metabolite of Ro. It was found that GGO attenuated tumor growth in immunocompromised mice undergoing heterograft transplantation by regulating MAPK signaling pathway and gut microbiota9. In this study, GGO significantly suppressed the proliferation of HeLa cells with an IC₅₀ value of 4.19 μM at 24 h (Fig. 1B), signifying a notably lower inhibitory concentration compared to ginsenoside Rg3 $(45 \,\mu\text{M} \text{ at } 24 \,\text{h})^{23}$ and Rh2 $(25 \,\mu\text{M} \text{ at } 24 \,\text{h})^{24}$ on cervical cancer cells. Furthermore, GGO also suppressed the colony forming ability of HeLa cells in a dose-dependent manner and blocked cell cycle progression at the G0/G1

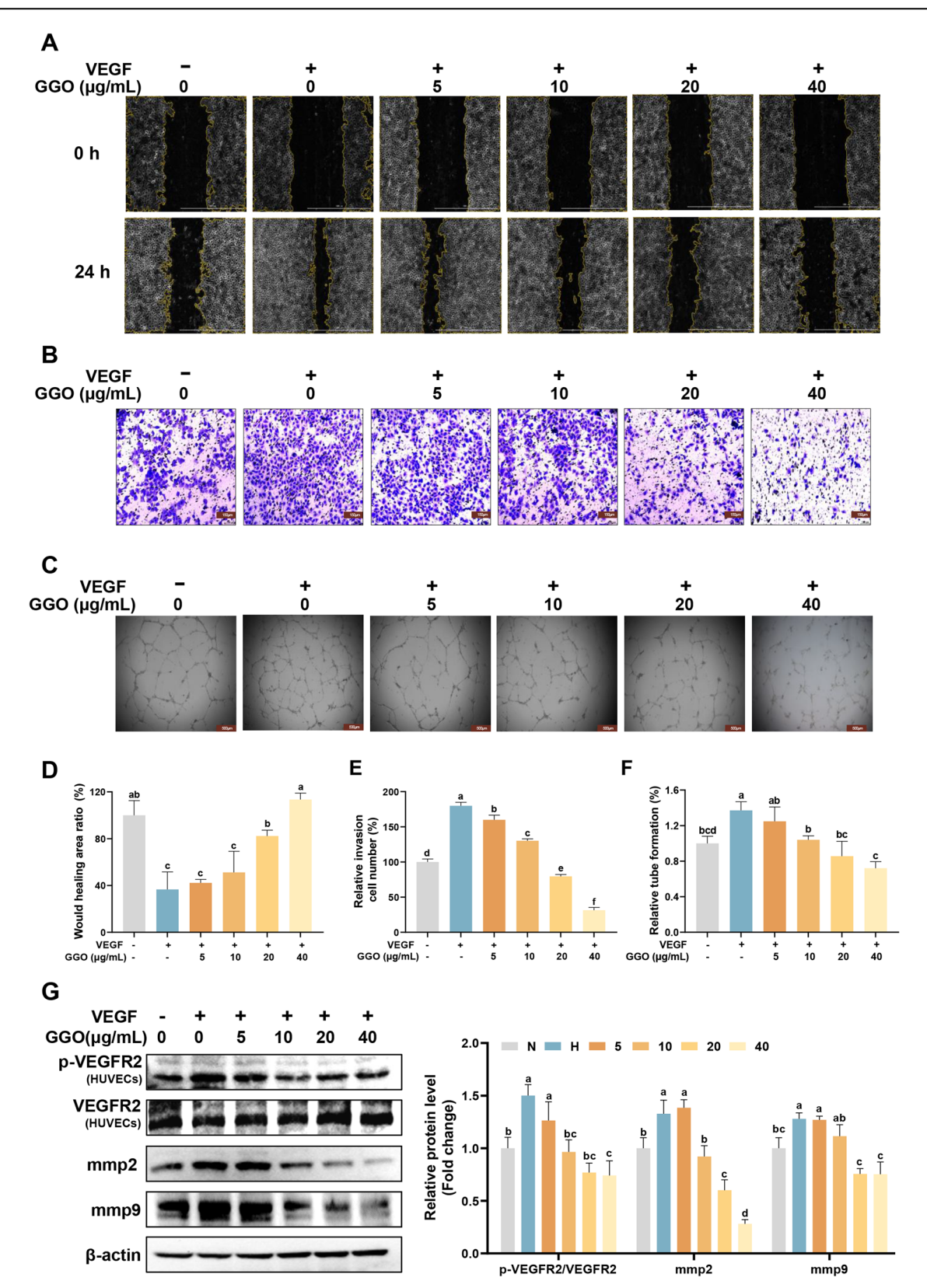


Fig. 4 | GGO inhibited the process of angiogenesis in HUVECs by interfering VEGF/VEGFR2 paracrine pathway. A The inhibition of GGO on the migration of HUVECs induced by VEGF (20 ng/mL) was revealed by Wound healing assay, and the scratches were pictured at 0 and 24 h (scale bars at 1000 μ m). B Inhibitory effects of GGO on the invasion of HUVECs induced by VEGF (20 ng/mL) were detected by the Transwell invasion assay. (scale bars at 100 μ m). C The inhibitory effects of GGO on the tube formation of HUVECs were indicated by culturing HUVECs induced by

VEGF on Matrigel (20 ng/mL) (scale bars at 500 µm). The relative (**D**) scratch area, (**E**) invasion cell numbers and (**F**) tube branching points were analyzed by ImageJ software. **G** The expressions of VEGFR2, p-VEGFR2, mmp2, and mmp9 in HUVECs induced by VEGF (20 ng/mL) following GGO treatment. (**D**) The relative intensities of these protein bands were analyzed by the ImageJ software, β -actin served as a loading control. Values were represented as means \pm SD (n = 3). Different letters indicated the significant differences between different groups (p < 0.05).

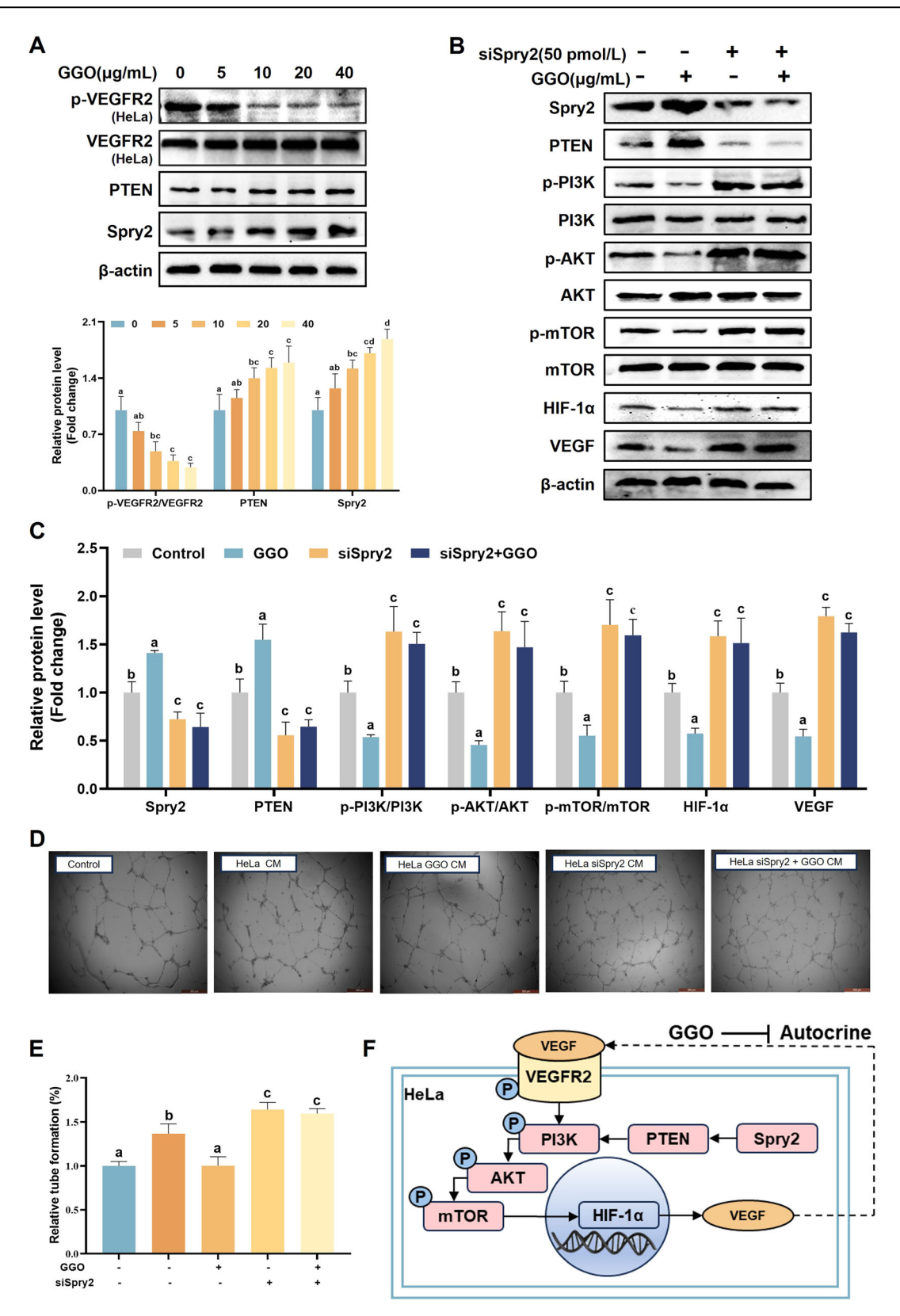
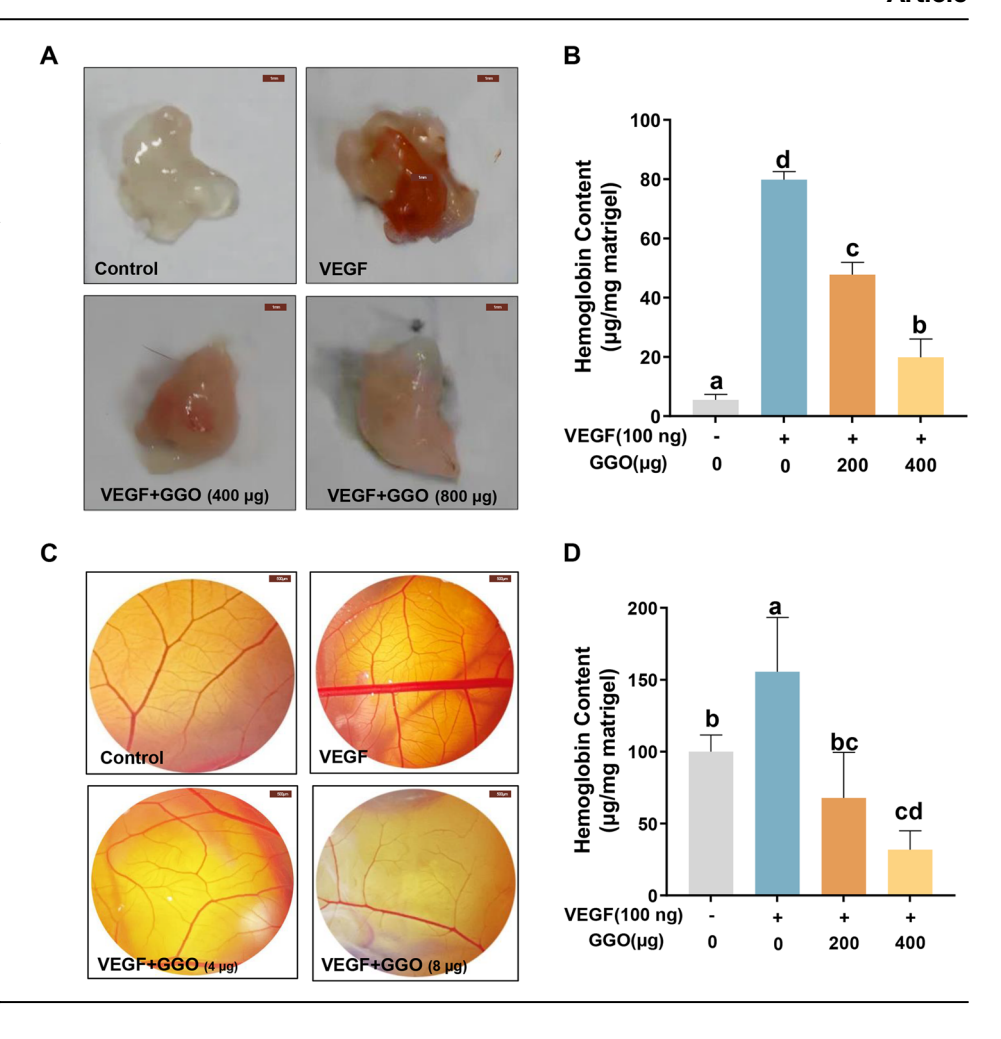


Fig. 5 | Effects of GGO on VEGF/VEGFR2 autocrine axis by activating Spry2 in HeLa cells. A The expressions of VEGFR2, p-VEGFR2, Spry2 and PTEN in HeLa cells after GGO treatment. B The expressions of Spry2, PTEN, p-PI3K, PI3K, p-AKT, AKT, mTOR, p-mTOR, HIF-1 α and VEGF in HeLa cells which were silenced Spry2 and treated with or without GGO (20 μ g/mL). C The relative intensities of these protein bands were analyzed by the ImageJ software, β -actin served as a loading

control. **D** The effect of CM from HeLa cells which were silenced Spry2 or not and combined with or without GGO (20 μ g/mL) on tube formation of HUVECs. **E** The relative branching points were analyzed by ImageJ software. **F** Mechanism diagram of GGO inhibiting VEGF/VEGFR2 autocrine axis. Values were represented as means \pm SD (n = 3). Different letters indicated the significant differences between different groups (p < 0.05).

Fig. 6 | Effects of GGO on angiogenesis in vivo. A The Matrigel plugs containing with or without GGO (200 or 400 μ g) and VEGF (100 ng/mouse) were harvested after 14 d. B Hemoglobin content in Matrigel plugs was measured by Hemoglobin (Hb) content assay kit. Anti-angiogenesis effects of GGO in CAM. C The representative images of new blood vessels were photographed after GGO (4 or 8 μ g) combined with or without VEGF (100 ng/egg) treatment for 72 h and (D) quantified by Image J software. Values were represented as means \pm SD (n = 6). Different letters indicated the significant differences between different groups (p < 0.05).



phase, indicating its inhibitory effect on proliferation (Fig. 1C–F). Although natural compounds such as paclitaxel and vincristine have been approved for cervical cancer treatment, their efficacy was limited due to their toxic side effects^{25,26}. GGO significantly impeded the growth of HeLa xenografted mice tumors, without adverse impact on liver, kidneys and other vital organs (Fig. 7B, C and S2). Therefore, GGO has shown advantages in inhibiting cervical cancer both in vivo and in vitro, thus showing potential as an ingredient of anti-cancer functional food.

Hypoxia is a prevalent hallmark in micro environment of many cancer types. The activation of HIF-1a represents the predominant pathway employed by tumor cells to survive and proliferate in low oxygen tension conditions^{14,15}. Under hypoxic conditions, HIF-1α is stably activated and translocated into the nucleus, to combine with hypoxia response elements in numerous genes that play crucial roles in energy homeostasis, angiogenesis, as well as the regulation of cell survival and proliferation 16. Therefore, HIF-1α was considered as an independent risk factor affecting tumor prognosis, and several HIF-1a inhibitors have been approved for clinical use or completed preclinical trials, such as YC-1, PX-478, and 2-Methoxyestradiol^{15,27}. This study found that GGO inhibited the expression and nuclear translocation of HIF-1a under hypoxia conditions (Fig. 2A-E). PI3K/AKT/mTOR pathway is the most commonly dysregulated and signaling pathway in human cancer, which has a wide range of effects on basic cell functions, such as metabolism, proliferation and cell survival. It also a well-known upstream signaling pathway of HIF-1a, which principally regulate HIF-1a through control transcription, translation, and activity¹³. There were several ginsenosides (such as Rg3, Rh2, Rg5) that exhibited anti-tumor effects in cervical cancer, which were related to their effects on the PI3K/AKT signaling pathway²⁸. GGO also inhibited the phosphorylation of PI3K, AKT, and mTOR under normoxia and hypoxia conditions (Fig. 2A-D). And, the effects of GGO on HIF-1 α expressions was abrogated when HeLa cells were pretreated with PI3K inhibitor LY294002 (Fig. 3C). These results indicated that GGO might inhibited the expression of HIF-1 α by blocking the PI3K/AKT signaling pathway, and played the role in suppressing tumor cell proliferation, which was consistent to the mechanism of native compound isorhamnetin (C16H12O7) and cryptotanshinone antitumor activity^{29,30}.

Tumor cells require angiogenesis delivering essential nutrients and oxygena to continuously proliferate³¹. Angiogenesis has been recognized as an independent risk factor and significant prognostic marker in cervical cancer³². Patients with a high tumor microvessel density had an increased risk to recurrent disease and lower overall survival³³. Therefore, blocking new vessel formation represented an attractive target for cancer therapy³⁴. VEGF is one of the essential growth factors which promotes cancer angiogenesis, and mainly regulated by HIF-1α¹⁶. Elevated serum VEGF in cancer patients serves as prognostic marker for enhanced tumor growth and metastatic dissemination, which is associated with disease progression, unfavorable outcomes and resistance to chemotherapy³¹. GGO significantly inhibited the VEGF expression in HeLa cells and HeLa xenograft tumor, as well as the VEGF level in the serum of HeLa heterologous xenograft tumor mice (Figs. 3A, B and 7D, E). When HeLa cells were pretreated with PI3K or HIF-1α inhibitors, (LY294002 and LW6) respectively, the GGO lost its inhibitory effect on VEGF expression, giving GGO the potential to inhibit angiogenesis (Fig. 3C, D). These results confirmed the ability of GGO to inhibit VEGF expression by blocking PI3K/AKT/HIF-1a signaling pathway, which gave GGO anti-angiogenesis potential.

In solid tumor, tumor cell-secreted VEGF binds to VEGFR2 on endothelial cell membrane, forming a receptor-ligand complex that undergoes endocytosis. This process promotes endothelial cell activation and increases vascular permeability, representing a paracrine mechanism of

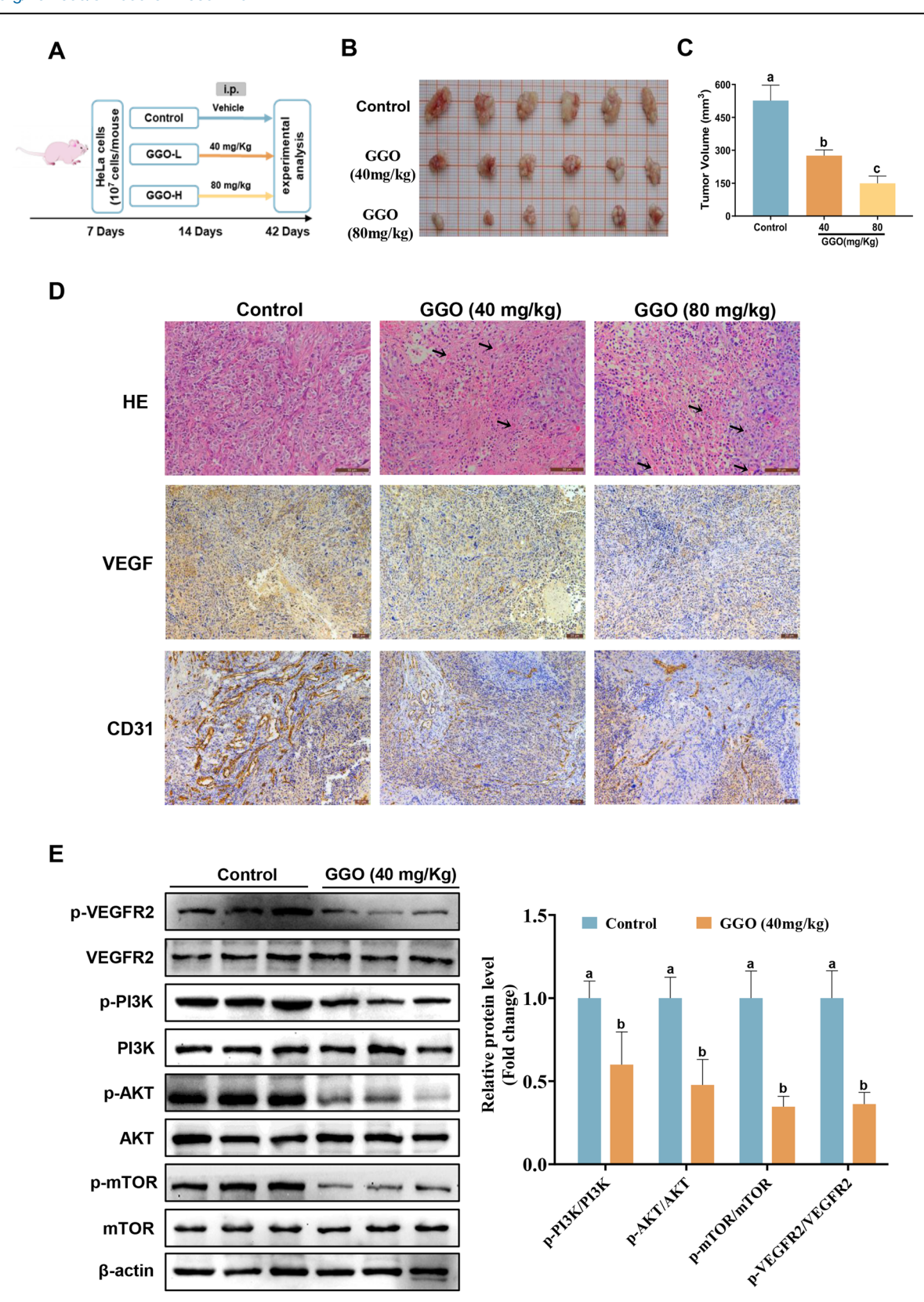


Fig. 7 | Effects of GGO on HeLa xenograft nude mice. A Animal experimental procedure. B Images of tumors in animal experiments. C The inhibition of GGO on tumor volume of tumor-bearing mice. D Representative H&E, VEGF and CD31 immunohistochemistry staining images of tumor issue. E Protein expression of

phosphorylated VEGFR2, PI3K, AKT and mTOR in tumor issue. The relative intensities of these protein bands were analyzed by the ImageJ software, β -actin served as a loading control. Values were represented as means \pm SD (n = 8). Different letters indicated the significant differences between different groups (p < 0.05).

the VEGF-VEGFR pathway¹⁸. VEGF and VEGFR2 have become important targets for developing antiangiogenic drugs (such as bevacizumab and sunitinib)35,36. This study showed that GGO reduces the secretion of VEGF in HeLa cells while inhibiting the phosphorylation activation of VEGFR2 induced by VEGF in HUVECs, thus blocking the paracrine pathway of VEGF/VEGFR2 (Figs. 3F and 4C). Angiogenesis, being a complex process, encompasses the proliferation, migration, and tubulogenic of endothelial cells, as well as the development and sprouting of novel capillary branches along with extracellular matrix degradation¹⁷. GGO significantly suppressed the proliferation, migration, invasion, and tube formation of VEGFstimulated HUVECs (Figs. S1B and 4A-F). GGO also suppressed the expressions of mmp2 and mmp9 in HUVECs (Fig. 4G), which are responsible for degrading the extracellular matrix (ECM). This inhibition ultimately promotes endothelial cell invasion and facilitates the formation of new blood vessels³⁷. The microvessels densities induced by VEGF was effectively reduced by GGO in both the CAM and Matrigel plug models, which are well-established systems for investigating tumor angiogenesis (Fig. 6A-D). In addition, GGO, at concentrations similar to Sunitinib (40 mg/Kg)³⁸and Sorafenib (50 mg/Kg)³⁹, resulted in the significant reduction of tumor blood vessel density in the HeLa xenografted mice (Fig. 7D). Excitingly, after GGO intervention, there were numerous hemorrhagic foci within the tumor, but none in the normal tissue (Fig. 7D and S2). It was consistent with the result that GGO inhibited the viability of VEGF-induced proliferative state HUVECS cells in vitro (representing endothelial cells in the tumor), but had no significant effect on the viability of resting state HUVECs cultured normally (representing endothelial cells in normal tissue) (Fig.4B and S1A). These results indicated that GGO has a targeted inhibitory effect on tumor angiogenesis, which provided a basis for its development as a health product. Previous studies showed that Zingibroside R1, Chikusetsusaponin IVa, Calenduloside E, OA, generated through hydrolyzing sugar groups linked to branched chains of Ro, which exhibited anti-angiogenic properties not observed in Ro alone⁷. This anti-angiogenic effect of GGO may be related to its similar chemical structure with other Ro metabolite, as differences in the position, type and number of sugar groups of ginsenosides lead to their unique pharmacological effects^{40,41}.

The latest research found that the expression of VEGFR2 was abnormally highly expressed in various solid tumors, including hepatocellular carcinoma, ovarian carcinoma and cervical cancers, which indicated the presence of the VEGF/VEGFR2 autocrine axis⁴². Notably, there was a significant increase (approximately 70%) in the positive rate of VEGFR2 staining in samples from cervical cancer patients, which was positively correlated with clinical tumor grade¹⁹. Autocrine VEGF/ VEGFR2 signaling has been recognized to contribute to tumorigenesis in angiogenesis-independent and -dependent manners. VEGF/VEGFR2 autocrine axis stimulated VEGF secretion, thus sustaining an autocrine feedback loop in tumor cells and stimulate angiogenesis 19,43. Besides, it promoted cancer cells proliferation and conferred apoptosis resistance⁴⁴. These effects of the VEGF/VEGFR2 autocrine axis are related to its downstream signaling, in which PI3K/AKT is the most critical signaling pathway¹⁸. Malekan et al. demonstrated that inhibition of the VEGF/ VEGFR2 autocrine axis resulted in decreased proliferation and increased apoptosis in the A375 malignant melanoma cell line in vitro, as well as suppressed angiogenesis and melanoma growth in vivo⁴⁵. This study has achieved similar results that GGO inhibited the phosphorylation activation of VEGFR2 and its downstream PI3K/AKT singling pathway in HeLa cells, thus inhibiting the expression of VEGF and proliferation of HeLa cells, which explained the dual inhibitory effect of GGO on angiogenesis and cell proliferation (Figs. 2A, B, 3C, 5A, F). Spry2 is an important negative regulator of VEGFR2 signal transduction, increasing the activation and stability of lipid phosphatase PTEN which negatively regulates the PI3K/AKT pathway via dephosphorylation of phosphatidylinositol 3-,4-,5-phosphate (PIP3)²⁰. By silencing Spry2 with siRNA, it was demonstrated that GGO inhibited the downstream PI3K/AKT/HIF-1a signaling of VEGFR2 by activating Spry2 (Fig. 5B, C). In addition, molecular docking results further indicated that Spry2 possibly was a potential target for GGO to exert the above dual inhibitory effects. Furthermore, preclinical research has shown that the EGFR and VEGF pathways cooperate to function as compensatory signaling pathways and support the long-term development of cancer cells. Furthermore, overexpression of EGFR is closely linked to acquired therapeutic resistance of VEGFR targeting drugs³⁴. Blocking the PI3K/AKT pathway prevents the treatment failure of GGO for angiogenesis due to drug resistance, because PI3K/AKT is the common pathway of VEGFR2 and EGFR signal transduction. The effect of CM of HeLa cells treated in different ways on the ability of inducing HUVECs to form tubes confirmed this mechanism that blocking of VEGFR2 autocrine axis can ensure the realization of the anti-angiogenic effects of GGO (Fig. 5D, E). These results provided more possibilities and opportunities for the development of anti-angiogenesis health food.

In summary, Sry2 probably was a potential target for GGO to play a dual role in inhibiting cervical cancer cell proliferation and angiogenesis. GGO inhibited the PI3K/AKT/HIF-1 α signaling pathway in the VEGF/VEGFR autocrine axis and the VEGF/VEGFR2 paracrine pathway by activating Spry2 (Fig. 8). Furthermore, the dual inhibitory action of GGO assisted in reducing the formation of tumors in immunocompromised mice receiving heterograft transplants. This study proved that GGO, as a natural compound extracted from ginseng, had significant anti-cervical cancer activity and low toxic side effects, which provided a theoretical basis for the development and utilization of GGO. In the future, by carrying out more indepth animal tests and clinical trials, GGO is expected to be developed into a functional food or drug against cervical cancer, bringing new hope to patients with cervical cancer.

Materials and methods Materials and reagents

Snailase was gained from Beijing Baierdi Biological Company (Beijing, China). RPMI 1640 medium, heat-inactivated fetal bovine serum (FBS), trypsin-EDTA (0.25%), and penicillin/streptomycin were purchased from Gibco Inc. (Grand Island, NY). Endothelial cell medium (ECM) was acquired from Science Cell Biotechnology (San Diego, California). 3-(4,5-Dimethyl-thiazol-2-yl)-2,5-diphenyltetrazolium bromide (MTT), LW6 (a HIF-1α inhibitor), cobaltous chloride (CoCl2), and sodium heparin were obtained from Solarbio Science&Technology Co., Ltd (Beijing, China). Growth factor reduced Matrigel was purchased from BD Biosciences (San Jose, CA, USA). Recombinant Human VEGF165 and insulin-like growth factor-1 (IGF-1) (a PI3K agonist) were procured from PeproTech Biotechnology Co., Ltd (Suzhou, China). LY294002 (a PI3K inhibitor), Lipo6000™ transfection reagent and cytotoxicity detection kit plus (LDH) were purchased from Beyotime Biotechnology co., Ltd (Shanghai, China). Enzyme-linked immunosorbent assay (ELISA) kits for Fibroblast Growth Factor (FGF), Epidermal growth factor (EGF), and vascular endothelial growth factor (VEGF) were provided by R&D Systems (Minneapolis). Radioimmunoprecipitation assay (RIPA) buffer and phenyl methane sulfonyl fluoride (PMSF) that used for cell protein extraction were obtain from Thermo Fisher Scientific (Waltham, Massachusetts, USA). Antibodies against phosphoinositide 3-kinase (PI3K), phospho-phosphoinositide 3kinase (p-PI3K), protein kinase B (AKT), phospho-protein kinase B (p-AKT), mammalian target of rapamycin (mTOR), and phospho- mammalian target of rapamycin (p-mTOR) were provided by Cell Signaling Technology (Boston, MA, USA). Antibodies against hypoxia-inducible factor-1α (HIF-1α), VEGF, sprouty RTK signaling antagonist 2 (SPRY2), phosphatase and tensin homolog deleted on chromosome ten (PTEN), platelet endothelial cell adhesion molecule-1 (CD31), β-actin, and HRP goat anti-rabbit IgG were purchased from Abcam Plc (Cambridge, UK).

Cell line and cell culture

HUVECs and HeLa cells were gained from the American Type Culture Collection (ATCC, Manassas, USA). HUVECs were cultured in endothelial cell medium (ECM) supplemented with 5% fetal bovine serum (FBS), 1% endothelial cell growth supplement (ECGS), and 1% antibiotics (penicillinstreptomycin). HeLa cells were grown in RIPA-1640 medium

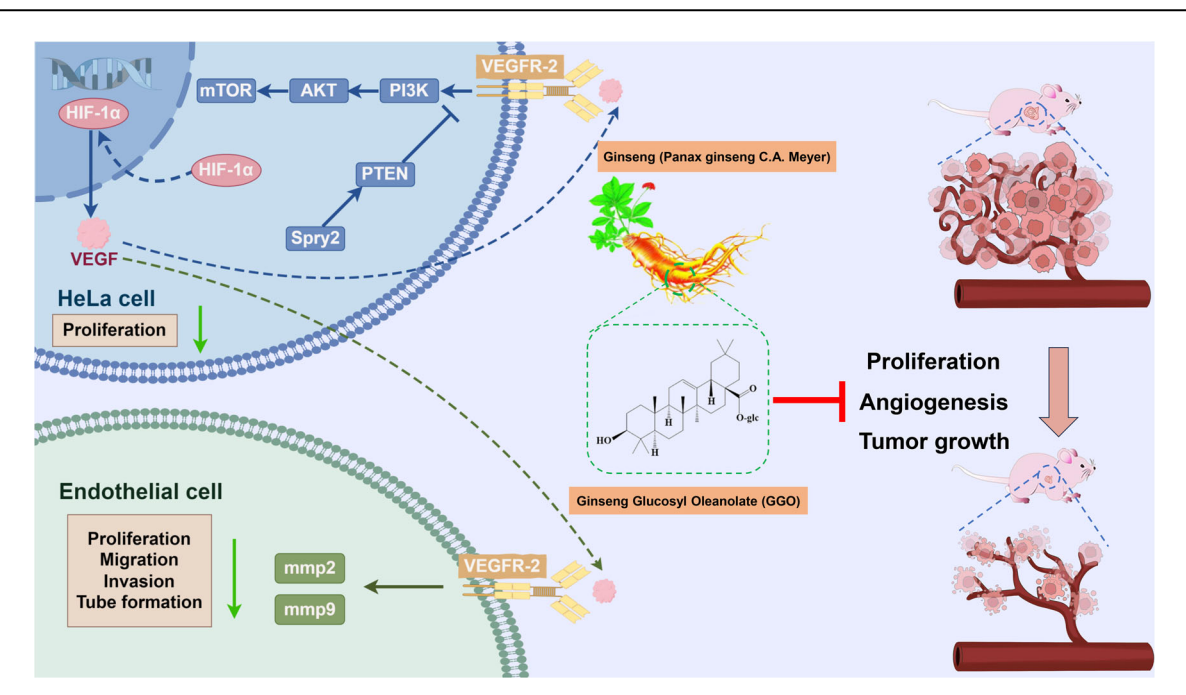


Fig. 8 | The mechanism of GGO inhibited cervical cancer cell proliferation and angiogenesis. Sry2 probably was a potential target for GGO to play a dual role in inhibiting cervical cancer cell proliferation and angiogenesis. GGO inhibited the

PI3K/AKT/HIF- 1α signaling pathway in the VEGF/VEGFR autocrine axis and the VEGF/VEGFR2 paracrine pathway by activating Spry2. Graphical abstract was created with Figdraw.

supplemented with 1% antibiotic and 10% FBS. Cobalt Chloride ($CoCl_2$) is a chemical inducer of hypoxia that was used in vitro to mimic hypoxia conditions. These cells were incubated at 37 °C with 5% CO_2 in a cell incubator.

Cell viability assay

HeLa cells and HUVECs were seeded at a density of 1×10^4 cells/well in 96-well plates, respectively, and incubated with various doses of GGO for either 24 h or 48 h. Following adding the thiazolyl blue tetrazolium bromide (MTT) solution (0.5 mg/mL), they were allowed to incubate at 37 °C for 4 h and protected from light. Finally, after dissolving the formazan crystals in dimethyl sulfoxide (DMSO), the absorbance was measured at 570 nm using a microplate reader (Tecan, Switzerland).

Lactate dehydrogenase (LDH) toxicity assay

The commercial LDH cytotoxicity assay kit was used to perform a cytotoxicity experiment based on LDH secretion. In summary, HUVECs were seeded in a 96-well plate (1×10^4 cells/well) and exposed to varying doses of GGO for 24 h. The supernatant was collected and centrifuged at 1200 g for 10 minutes. The concentrations of LDH were measured using the supernatant following the manufacturer's protocol.

Colony formation assay

HeLa cells (2000 cells/well) were seeded in a plate in each experimental group. After the cells adhered, the different concentrations of GGO (0, 5, 10, 20, 40 mg/mL) were added and cultured for 24 h. Then the cultures were maintained for a duration of 14 days with complete medium changes every 3 days. Then fixed with 4% paraformaldehyde and stained with 0.1% crystal violet. Allowing to dry, photographed under a camera and counted.

Wound healing assay

A 6-well plate was seeded with HUVECs (5×10^5 cells/well). When the cell monolayer was established, it was scratched with a $10 \,\mu\text{L}$ sterilized pipette tip to generate wound (n = 3), and then cell debris was removed by washing three times in phosphate buffered solution (PBS). Afterward, the medium containing various GGO concentrations with or without $20 \,\text{ng/mL}$ VEGF was applied. Photographs of the wound at $0 \,\text{and} \, 24 \,\text{h}$ were taken with an

inverted microscope (Leica, Wetzlar, Germany). ImageJ was used to quantify the areas of wounds.

Transwell invasion assay

Polycarbonate filters with 8 μm pores of the top chamber were pre-coated with 60 μL Matrigel, and used to seed HUVECs (5 \times 10^4 cells/well). The bottom chamber had 500 μL ECM containing 20% FBS and 20 ng/mL VEGF. Then the lower surface cells were fixed with 4% formaldehyde and stained with 0.1% crystal violet after incubating at 37 °C for 24 h. The invasion cells were counted and photographed under an inverted microscope.

Tube formation assay

A previously used assay for endothelial tube development on Matrigel was followed 46 . Briefly, a 96-well plate was pre-coated with 50 μL of Matrigel and let to polymerize for 30 min at 37 °C. Then HUVECs (2.5 \times 10 4 cells/well) were seeded on the Matrigel surface and cultured in fresh medium or condition medium (CM) to observe tube formation. The fresh medium had different doses of GGO and either 20 ng/mL VEGF or not. CM was made from culture supernatants, which were harvested from HeLa cells cultured with different concentrations of GGO. An inverted microscope was used to count the number of vessel branch points.

Enzyme-linked immunosorbent assay (ELISA)

The levels of VEGF, fibroblast growth factor (FGF), platelet-derived growth factor (PDGF) and epidermal growth factor (EGF) that secreted by HeLa cells were examined by commercial ELISA kits. Briefly, HeLa cells were seeded in a 6-well plate (1×10^6 cells/well) and given different doses of GGO to treat for 24 h. The supernatant was gathered and centrifuged for 10 min at 2000 g. The ELISA kits were used under the manufacturer's guidelines.

Small interfering RNA transfection

As directed by the manufacturer, HeLa cells were transfected for 48 h using Lipofectamine 6000TM. The synthetic Spry2 siRNA was produced by Comate Bioscience Co., Ltd. (Jilin, China), and the sequence was as follows: Spry2, 5' - GCAGGUACAUGUCUUGUCUTT - 3'. The knockdown was verified by Western blot analysis.

Chick chorioallantoic membrane (CAM) assay

Following the protocol outlined before, the CAM assay was conducted with slight modifications 47 . Fertilized chicken eggs (10 day old) were acquired from a neighboring hatchery. A 1 cm² window was cut, and then a 5 mm diameter sterile filter paper containing GGO (0, 4, and 8 µg) and with or without VEGF (100 ng), was applied to the CAM. After closing the air chamber, the incubation process was allowed to held for 72 h. Using the Image software, the numbers of blood vessel branch points were counted to quantify angiogenesis.

Matrigel plug assay

The animal tests followed the ethical rules of Medical Laboratory of Animal Center, Jilin Agricultural University's (No. 20190410005). The 500 μL 1:1 mixture of Matrigel: culture medium containing different concentrations of GGO (0, 400, 800 μg) and with or without heparin (20 U) and VEGF (100 ng) was administered subcutaneously into the left groin area of five-week-old male C57BL/6 mice. After 14 d, the mice were executed using cervical dislocation, meanwhile the Matrigel plugs were exposed. According to the manufacturer's instructions, the hemoglobin concentration was measured using the Drabkin reagent kit 525 to quantify the development of blood vessels.

Xenograft model in nude mouse

The design of animal experiments was shown in Fig. 7A. In short, five-week-old female BALB/c nude mice were kept at a constant temperature of 22 °C on a 12 h light-dark cycle with free access to food and water. After a week to acclimate and then received a subcutaneous injection of 1×10^6 HeLa cells in 200 μL sterile PBS in the right groin area. After the tumors had grown to a mean volume of 50 mm³, the mice were randomly divided into three groups of eight animals: The mice received intraperitoneal (ip) injections of GGO or normal saline once a day. After 21 d, the mice were executed using cervical dislocation and the xenografts were removed, and fixed in 4% paraformaldehyde.

Western blot analysis

In brief, the RIPA solution containing phenyl methane sulfonyl fluoride (PMSF) was used to obtain total protein. The protein concentration was measured using a BCA protein assay kit. An equal amount of protein was separated by sodium dodecyl sulfate-polyacrylamide gel electrophoresis (SDS-PAGE) and transferred to polyvinylidene difluoride (PVDF) membranes. Following incubation with the relevant primary and secondary antibodies, the protein was visualized using an image scanner (iBright, Thermo Fisher Scientific). Using ImageJ software, the protein levels were measured and normalized to $\beta\text{-actin}$.

Immunohistochemical analysis

Tumors were formalin-fixed and paraffin-embedded before being sliced into 5 μ m thick slices. The slices were treated with platelet endothelial cell adhesion molecule (CD31) and VEGF antibodies, and processed sequentially with goat anti-rabbit lgG secondary antibody. Additionally, slices were re-stained with hematoxylin and DAB. An inverted microscope was used for analysis and photographs.

Statistical analysis

The data were analyzed using the one-way analysis of variance (ANOVA) and represented as means \pm standard deviation (SD) using the Prism 8.0 software package. Differences between groups were considered significant at P < 0.05.

Data availability

All data generated or analyzed during this study are included in this published article and its Supplementary Information file.

Received: 9 August 2024; Accepted: 13 November 2024; Published online: 19 December 2024

References

- Qi, L. W., Wang, C. Z. & Yuan, C. S. Isolation and analysis of ginseng: advances and challenges. *Cheminform* 28, 467–495 (2011).
- Yao, W. & Guan, Y. Ginsenosides in cancer: A focus on the regulation of cell metabolism. *Biomed. Pharmacother.* 156, 113756 (2022).
- Yang, W. Z., Hu, Y., Wu, W. Y., Ye, M. & Guo, D. A. Saponins in the genus Panax L. (Araliaceae): A systematic review of their chemical diversity. *Phytochemistry* 106, 7–24 (2014).
- 4. Shah, M. A. et al. Ginsenosides in cancer: Targeting cell cycle arrest and apoptosis. *Chem. -Biol. Interact.* **382**, 110634 (2023).
- Lin, Z. et al. Recent progress (2015–2020) in the investigation of the pharmacological effects and mechanisms of ginsenoside Rb1, a main active ingredient in Panax ginseng Meyer. J. Ginseng Res. 46, 39–53 (2022).
- Xu, H. L., Chen, G. H., Wu, Y. T., Xie, L. P. & Zhou, Y. C. Ginsenoside Ro, an oleanolic saponin of Panax ginseng, exerts anti-inflammatory effect by direct inhibiting toll like receptor 4 signaling pathway. *J. Ginseng Res.* 46, 156–166 (2021).
- Zheng, S. W., Xiao, S. Y., Wang, J., Hou, W. & Wang, Y. P. Inhibitory Effects of Ginsenoside Ro on the Growth of B16F10 Melanoma via Its Metabolites. *Molecules* 24, 2985 (2019).
- 8. Wang, J. et al. Profiling and identification of the metabolites of ginsenoside Ro in rat faeces and urine after oral administration. *Eur. Food Res. Technol.* **242**, 199–210 (2016).
- Ai, Z. et al. Ginseng Glucosyl Oleanolate from Ginsenoside Ro, Exhibited Anti-Liver Cancer Activities via MAPKs and Gut Microbiota In Vitro/Vivo. J. Agric. Food Chem. 72, 7845–7860 (2024).
- Wan, Q. et al. Alkaloids from Piper longum Exhibit Anti-inflammatory Activity and Synergistic Effects with Chemotherapeutic Agents against Cervical Cancer Cells. J. Agric. Food Chem. 71, 10349–10360 (2023).
- Marchetti, C., Fagotti, A., Tombolini, V., Scambia, G. & De Felice, F. Survival and toxicity in neoadjuvant chemotherapy plus surgery versus definitive chemoradiotherapy for cervical cancer: A systematic review and meta-analysis. Cancer Treat. Rev. 83, 101945 (2020).
- Kashyap, A. et al. Quantification of tumor heterogeneity: from data acquisition to metric generation. *Trends Biotechnol.* 40, 647–676 (2022).
- Gao, T., Zhang, X., Zhao, J., Zhou, F. & Liu, S. SIK2 promotes reprogramming of glucose metabolism through PI3K/AKT/HIF-1α pathway and Drp1-mediated mitochondrial fission in ovarian cancer. Cancer Lett. 469, 89–101 (2019).
- Chen, D. et al. In vivo real-time monitoring of the development of hypoxia and angiogenesis in cervical cancer. *Chem. Eng. J.* 473, 145498 (2023).
- 15. Tang, W. & Zhao, G. Small molecules targeting HIF-1α pathway for cancer therapy in recent years. *Bioorg. Medicinal Chem.* **28**, 115235 (2020).
- Zhao, Y., Xing, C., Deng, Y., Ye, C. & Peng, H. HIF-1α signaling: Essential roles in tumorigenesis and implications in targeted therapies. *Genes Dis.* 11, 234–251 (2024).
- Wang, S. et al. Ethyl cinnamate suppresses tumor growth through anti-angiogenesis by attenuating VEGFR2 signal pathway in colorectal cancer. *J. Ethnopharmacol.* 326, 117913 (2024).
- Hu, W.-H. et al. Binding of Resveratrol to Vascular Endothelial Growth Factor Suppresses Angiogenesis by Inhibiting the Receptor Signaling. J. Agric. Food Chem. 67, 1127–1137 (2019).
- 19. Longatto-Filho, A. et al. Molecular characterization of EGFR, PDGFRA and VEGFR2 in cervical adenosquamous carcinoma. *BMC Cancer* **9**, 212 (2009).
- Edwin, F., Singh, R., Endersby, R., Baker, S. J. & Patel, T. B. The Tumor Suppressor PTEN Is Necessary for Human Sprouty 2-mediated Inhibition of Cell Proliferation. J. Biol. Chem. 281, 4816–4822 (2006).
- Pradhan, P. et al. Prospective Cohort Study of Ginseng Consumption in Association with Cancer Risk: Shanghai Women's Health Study. *J. Nutr.* 153, 1170–1177 (2023).
- Xu, W. et al. Preparation and bioactivity of the rare ginsenosides Rg3 and Rh2: An updated review. Fitoterapia 167, 105514 (2023).

- 23. Bian, S. et al. 20(S)-Ginsenoside Rg3 Promotes HeLa Cell Apoptosis by Regulating Autophagy. *Molecules* **24**, 3655 (2019).
- Liu, Y. et al. Ginsenoside Rh2 Induces HeLa Apoptosis through Upregulating Endoplasmic Reticulum Stress-Related and Downstream Apoptotic Gene Expression. Molecules 27, 7865 (2022).
- Khaiwa, N. et al. Camptothecin's journey from discovery to WHO Essential Medicine: Fifty years of promise. *Eur. J. Medicinal Chem.* 223, 113639 (2021).
- Symonds, R. P. et al. Cediranib combined with carboplatin and paclitaxel in patients with metastatic or recurrent cervical cancer (CIRCCa): a randomised, double-blind, placebo-controlled phase 2 trial. *Lancet Oncol.* 16, 1515–1524 (2015).
- Ouyang, C. et al. Advances in antitumor research of HIF-1α inhibitor YC-1 and its derivatives. *Bioorg. Chem.* 133, 106400 (2023).
- 28. Kang, B. W. & Chau, I. Molecular target: pan-AKT in gastric cancer. ESMO Open 5, e000728 (2020).
- Zhang, L. et al. Cryptotanshinone inhibits the growth and invasion of colon cancer by suppressing inflammation and tumor angiogenesis through modulating MMP/TIMP system, PI3K/Akt/mTOR signaling and HIF-1α nuclear translocation. *Int. Immunopharmacol.* 65, 429–437 (2018).
- Biswas, P. et al. The experimental significance of isorhamnetin as an
 effective therapeutic option for cancer: A comprehensive analysis.

 Biomedicine Pharmacother. 176, 116860 (2024).
- Dewangan, J. et al. Salinomycin inhibits breast cancer progression via targeting HIF-1α/VEGF mediated tumor angiogenesis in vitro and in vivo. Biochemical Pharm. 164, 326–335 (2019).
- 32. Folkman, J. Tumor angiogenesis: therapeutic implications. *N. Engl. J. Med.* **285**, 1182 (1971).
- Monk, B. J., Willmott, L. J. & Sumner, D. A. Anti-angiogenesis agents in metastatic or recurrent cervical cancer. *Gynecologic Oncol.* 116, 181–186 (2010).
- Gacche, R. N. Changing landscape of anti-angiogenic therapy: Novel approaches and clinical perspectives. *Biochimica et. Biophysica Acta* (BBA) - Rev. Cancer 1878, 189020 (2023).
- Person, F. et al. Bevacizumab-associated glomerular microangiopathy. Nat. Publ. Group. 32, 684–700 (2019).
- Tan, S. et al. TIE2-high cervical cancer cells promote tumor angiogenesis by upregulating TIE2 and VEGFR2 in endothelial cells. Transl. Oncol. 26, 101539 (2022).
- 37. Ren, A. et al. Endothelial GATA5 positively regulates angiogenesis via cathepsin S-mediated Angpt2/Flk1 and MMP2/9 signaling pathways. *Biochem. Biophys. Res. Commun.* **609**, 111–118 (2022).
- Maione, F., Capano, S., Regano, D., Zentilin, L. & Giraudo, E. Semaphorin 3A overcomes cancer hypoxia and metastatic dissemination induced by antiangiogenic treatment in mice. *J. Clin. Invest* 122, 1832 (2012).
- Chaudary, N., Hedley, D. W. & Hill, R. P. Orthotopic xenograft model of cervical cancer for studying microenvironmental effects on metastasis formation and response to drug treatment. *Curr. Protoc. Pharmacol.* 53, 14–19 (2011).
- Zhu, Y. et al. Ginsenoside Rh2 suppresses growth of uterine leiomyoma in vitro and in vivo and may regulate ERa/c-Src/p38 MAPK activity. J. Funct. Foods 18, 73–82 (2015).
- Li, X.-L. et al. Effect of ginsenoside CK combined with cisplatin on the proliferation and migration of human cervical cancer HeLa cells via Ras/ERK/MAPK pathway. J. Funct. Foods 102, 105438 (2023).
- Lichtenberger, B. M. et al. Autocrine VEGF Signaling Synergizes with EGFR in Tumor Cells to Promote Epithelial Cancer Development. *Cell* 140, 268–279 (2010).
- Bonsang, B. et al. VEGF and VEGFR family members are expressed by neoplastic cells of NF1-associated tumors and may play an oncogenic role in malignant peripheral nerve sheath tumor growth through an autocrine loop. Ann. Diagnostic Pathol. 60, 151997 (2022).

- Peng, S. et al. Intracellular autocrine VEGF signaling promotes EBDC cell proliferation, which can be inhibited by Apatinib. *Cancer Lett.* 373, 193–202 (2016).
- 45. Malekan, M. et al. VEGF/VEGFR axis and its signaling in melanoma: Current knowledge toward therapeutic targeting agents and future perspectives. *Life Sci.* **345**, 122563 (2024).
- Haraguchi, T. et al. Cecal Succinate Elevated by Some Dietary Polyphenols May Inhibit Colon Cancer Cell Proliferation and Angiogenesis. J. Agric. Food Chem. 62, 5589–5594 (2014).
- García-Vilas, J. A., Quesada, A. R. & Medina, M. Á.
 4-Methylumbelliferone Inhibits Angiogenesis in Vitro and in Vivo. J. Agric. Food Chem. 61, 4063–4071 (2013).

Acknowledgements

This work was supported by the Key R&D Program of Jilin Provincial Department of Science and Technology (20210204040YY). Graphical Abstract was created with Figdraw.

Author contributions

Writing – original draft, Validation, Investigation, Formal analysis, S.T.L.; Validation, Investigation, Formal analysis, Z.Y.A.; Validation, Investigation, Formal analysis, Y.H.; Methodology, J.S.Z. Validation, P.T.; Methodology, H.Y.Z.; Methodology, G.Q.R.; Supervision, Resources, X.L.; Funding acquisition, Y.W.; Funding acquisition, B.N.; Writing – review & editing, Supervision, Resources, Project administration, Funding acquisition, Conceptualization, Y.H.W.

Competing interests

The authors declare that they have no known competing financial interests or personal relationships that could have appeared to influence the work reported in this paper.

Additional information

Supplementary information The online version contains supplementary material available at https://doi.org/10.1038/s41538-024-00341-3.

Correspondence and requests for materials should be addressed to Yuhua Wang.

Reprints and permissions information is available at http://www.nature.com/reprints

Publisher's note Springer Nature remains neutral with regard to jurisdictional claims in published maps and institutional affiliations.

Open Access This article is licensed under a Creative Commons Attribution-NonCommercial-NoDerivatives 4.0 International License, which permits any non-commercial use, sharing, distribution and reproduction in any medium or format, as long as you give appropriate credit to the original author(s) and the source, provide a link to the Creative Commons licence, and indicate if you modified the licensed material. You do not have permission under this licence to share adapted material derived from this article or parts of it. The images or other third party material in this article are included in the article's Creative Commons licence, unless indicated otherwise in a credit line to the material. If material is not included in the article's Creative Commons licence and your intended use is not permitted by statutory regulation or exceeds the permitted use, you will need to obtain permission directly from the copyright holder. To view a copy of this licence, visit https://creativecommons.org/licenses/by-nc-nd/4.0/.

© The Author(s) 2024, corrected publication 2025